Analysis and Design of Hybrid Harmonic Suppression Scheme for VSG Considering Nonlinear Loads and Distorted Grid

Lou, Guannan; Yang, Quan; Gu, Wei; Quan, Xiangjun; Guerrero, Josep M.; Li, Shanlin

Published in:
IEEE Transactions on Energy Conversion

DOI (link to publication from Publisher):
10.1109/TEC.2021.3063607

Publication date:
2021

Document Version
Accepted author manuscript, peer reviewed version

Analysis and Design of Hybrid Harmonic Suppression Scheme for VSG Considering Nonlinear Loads and Distorted Grid

Guannan Lou, *Member, IEEE,* Quan Yang, Wei Gu, *Senior Member, IEEE,* Xiangjun Quan, and Josep M. Guerrero, *Fellow, IEEE,* Shanlin Li

***Abstract*—The power quality of virtual synchronous generator (VSG) inevitably deteriorates in the presence of local nonlinear loads and distorted grid. In this paper, the conflict involved in the simultaneous elimination of distortion for both the inverter local load voltage and the grid exchanged current is first described. A unified control structure is presented that enables a tunable tradeoff between the two constrained harmonic sources. Then, a hybrid harmonic suppression scheme is proposed to enable the further improvement of the adaptability of VSG, which mainly consists of a local voltage harmonic control loop and an adaptive grid current-controlled loop. The local voltage harmonic control loop aims to scale down the inverter output impedance via a negative feedback loop, while the grid current-controlled compensator is intended to counteract the adverse effects from a weak grid via an additional voltage, which leads to substantially lower total harmonic distortion for both the local load voltage and the grid current at the same time. Small-signal modelling is performed to investigate the system stability and its robustness to parameter perturbations. The effectiveness of the proposed methodology is verified using hardware-in-the-loop simulations.**

***Index Terms*—Distorted grid, harmonic suppression, harmonic observer, nonlinear load, virtual synchronous generator.**

I. Introduction

Nowadays, with the rapidly expanding penetration of distributed generations (DGs), power systems are developing towards a more distributed and power-electronics-interfaced paradigm. These electrical converters facilitate the flexible operation of DGs, but they also pose severe challenges to the system stability and controllability because of their inertia-less characteristics. Therefore, the concept of virtual synchronous generator (VSG), which simulates the rotor inertia and droop features of synchronous generators in DG applications, has emerged and gained popularity [1]-[3]. Various researches have been undertaken on VSG with regard to aspects including the VSG principle and classification [3], [4], virtual inertia and dynamic performance [5]-[7], stability analyses [8], [9], and parameter optimization [10]. As a meliorated means conducive to environmentally friendly DGs, VSG is desired to play a vital role in supplying high-quality power to both the main grid and local loads.

Generally, power-electronics-interfaced DGs are located within an identifiable electrical boundary, where the grid can be easily distorted by the increased permeability of generations because of the pulse-width modulation (PWM) and switching behavior. Besides, intensive use of nonlinear loads can cause serious harmonic currents even if a purely sinusoidal voltage is supplied. Harmonics from distorted grid and nonlinear load lead to power quality issues, e.g. overheating, power losses, and mechanical vibrations, which restrict the VSG applications in the renewable energy field. Therefore, stringent schemes must be used to guarantee that the total harmonic distortions (THD) for both local voltage and grid current are low, below 5% in line with industrial requirements [11] or, in the best scenario, eliminated entirely.

Given that most of existing literature on VSG addresses the improvement of dynamic performance and few account for power quality concerns, the corresponding research on inverter-related droop control can be regarded as reference because both research directions pertain to power electronics. The traditional method to restrain harmonic currents was to install passive filter or active power filter (APF), which acted as harmonic conductances [12], [13]. In [14], [15], a control scheme was proposed based on the introduction of distorted currents into the current reference, which is subject to the dispersion features of DGs and high-precision measurement. An active branch method based on voltage feed-forward control was introduced to suppress harmonic currents drastically, with the harmonic impedance increased [16]. For harmonic voltage suppression, a harmonic droop controller was proposed in [11] by adding the harmonic voltage from Fourier analysis to the inverter voltage reference, with limited improved results. Considering that the output impedance can play a critical role in attenuating THD, a virtual capacitive impedance was added in [17], [18], to counteract the harmonic voltage drop. In [19], an approach to abate the inverter output impedance via a negative feedforward was presented with most of load harmonic currents absorbed by inverters. Additionally, several control schemes based on multiple proportional resonance [20], [21], deadbeat hysteresis [22], repetitive control [23] and internal model principle [24] were used to restrain harmonic voltage and current with complex implementation.

Stated thus, it is not difficult to achieve low THD for either

This work was supported in part by the National Science Foundation of China under Grant 52007031, the National Science Foundation of Jiangsu Province under Grant BK20200404, the National Key R&D Program of China under Grant 2016YFB0900404, the Fundamental Research Funds for the Central Universities and Project Funding for Jiangsu Provincial Key Laboratory of Smart Grid Technology and Equipment, Southeast University. (corresponding author: wgu)

G. Lou, W. Gu, X. Quan, and S. Li are with the School of Electrical Engineering, Southeast University, Nanjing, Jiangsu 210096, China. G. Lou is also with the Jiangsu Provincial Key Laboratory of Smart Grid Technology and Equipment, Southeast University. (glou@seu.edu.cn, wgu@seu.edu.cn)

Q. Yang is with the School of Electrical Engineering, Southeast University, Nanjing, Jiangsu 210096, China and Dongguan Power Supply Bureau of Guangdong power grid company, Guangdong 523000, China.

J. M. Guerrero is with the Center for Research on Microgrids (CROM), Department of Energy Technology, Aalborg University, 9220 Aalborg East, Denmark. (Tel: +45 2037 8262; Fax: +45 9815 1411; e-mail: joz@et.aau.dk)

This article has been accepted for publication in a future issue of this journal, but has not been fully edited. Content may change prior to final publication. Citation information: DOI 10.1109/TEC.2021.3063607, IEEE Transactions on Energy Conversion

the inverter local voltage or grid current; however, no strategy has been devoted to low THD for both the local voltage and grid current simultaneously in the presence of nonlinear loads and distorted grid because the combination of goals appears infeasible. Specifically, it is advantageous for the nonlinear load current flowing into VSG side when the output harmonic impedance is expected to be small, but the harmonic component in grid current would be correspondingly enlarged, or vice versa. Few research efforts have been geared toward the quantitative analysis of the fundamental limitation. As stated in [25], the power quality concerns of VSG in the dual harmonic sources are more troublesome than those of inverters because of the VSG dynamic characteristics in the harmonic domain. To the best of our knowledge, an impedance-based harmonic suppression scheme for VSG was proposed without closed-loop control in case of nonlinear loads and weak grid [26], whereas its robustness to nonlinear load variation was unsatisfactory due to the parameter-dependency of feed-forwards. Given that critical loads are sensitive to the local voltage quality, an appropriate control scheme is required to address both the inverter local voltage and grid current simultaneously in case of two harmonic scenarios.

Motivated by the research gap described above, this paper investigates the contradiction of concurrent harmonic inhibition for both nonlinear loads and distorted grid quantitatively. A hybrid harmonic suppression scheme is then proposed with a tunable tradeoff and complete manner for harmonic sources. Using a small-signal model, the dynamics of proposed scheme are analyzed. The study contributions are listed below.

(1) In this paper, deriving the fundamental limitation of VSG harmonic inhibition in presence of distorted grid and nonlinear loads, a unified harmonic control structure is presented with a tunable tradeoff between the two constrained harmonic sources.

(2) A hybrid harmonic suppression method is proposed to enable the complete suppression of the dual distortions through a local voltage feedback control loop and adaptive grid current compensation, which can attenuate the harmonics remarkably and guarantee a high-quality power supply for VSG.

(3) A multiple harmonic sequence components observer (MHSCO) [27] is introduced to enable the accurate and exhaustive detection of individual harmonics simultaneously.

This paper begins with a brief review of power quality with distorted grid and local nonlinear loads in Section II. Section III elaborates on the conflict of total harmonic suppression. A hybrid harmonic suppression scheme is proposed in Section IV, with stability analysis. Section VI presents hardware-in-the-loop (HIL) simulations and Section VII summarizes this study.

II. Review of VSG Harmonic Suppression

A. VSG Control Scheme

The topological structure of the inverter-interfaced DG is depicted in Fig. 1, where the inverter behaves as a voltage-controlled VSG [1], [3], and both linear and nonlinear loads are located at the point of common coupling (PCC). PCC is connected to main grid with a static switch (STS), by which the operation mode of DG can be decided. R_f, L_f, and C_f are the filter resistance, inductance and capacitance, respectively; Z_g denotes the grid impedance, mainly inductive characteristic dominated; Z_{line} denotes the line impedance between the inverter and PCC; u_{VSG} and i_i are the inverter voltage and current, respectively; u_o and i_o are the output voltage and current, respective; u_g and i_g represent the grid voltage and current, respectively; i_{Load1} and i_{Load2} are the currents of the linear and nonlinear loads. Note that dc bus dynamics of primary power source can be ignored, with a reasonable assumption of an ideal dc voltage U_{dc} [28].

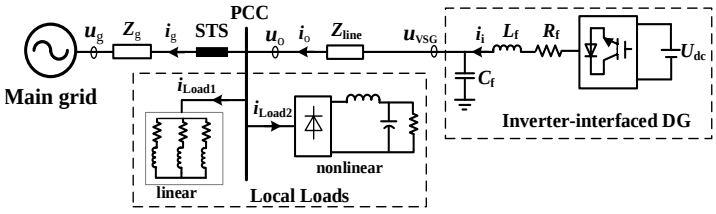

Fig. 1. Structural diagram of grid-connected DG

A thorough survey of VSG control scheme is beyond the scope of this paper, with the fundamental principle [8], [29] in Fig. 2, where the inertial coefficient J and damping factor D are introduced to emulate the moment of inertia and power oscillation damping, respectively; P_n and ω_n are the rated active power and frequency, respectively; Q_n and U_n are the rated reactive power and rated voltage, respectively; k_u denotes the Q-U droop coefficient and K is adjusted for the superior dynamics of reactive power. The power controller regulates the output reference voltage E and phase angle θ based on the local powers P and Q. u_o^* represents the output voltage reference and the cascaded voltage current controller is formulated to achieve no steady-state tracking error. The subscript abc (resp. dq) denotes the relevant variables in the abc (resp. dq) frame.

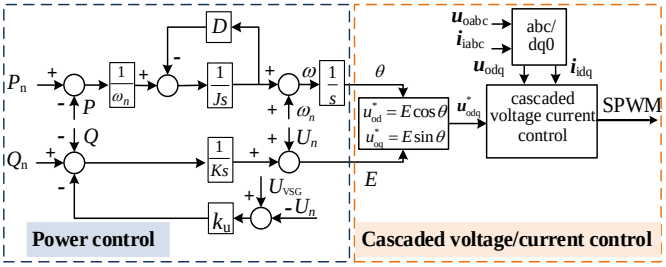

Fig. 2. Typical control block diagram of VSG

B. Problem Statement

The increased use of nonlinear loads and distorted grids will cause serious power quality issues for VSG in grid-connected operation. The equivalent harmonic-domain circuit is depicted in Fig. 3, where the superscript h is the harmonic component of variable and Z_{line} is considered to be zero in this paper because of short lines used. Note that the nonlinear load and distorted grid are denoted by harmonic current source i_L^h and voltage source u_g^h, respectively, while the VSG acts as a short circuit and a harmonic current exists due to the harmonic output impedance Z_o^h. Z_g^h represents the harmonic grid impedance.

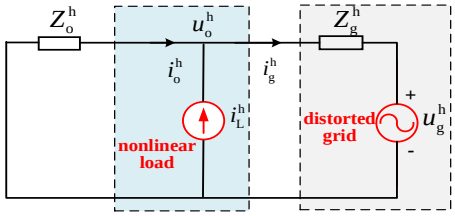

Fig. 3. Circuit of the harmonic-domain

Hence, the h-th harmonic output voltage u_o^h and grid harmonic current i_g^h of VSG under study can be expressed as

$$\begin{cases} u_o^h = \dfrac{Z_o^h Z_g^h}{Z_o^h + Z_g^h} i_L^h + \dfrac{Z_o^h}{Z_o^h + Z_g^h} u_g^h \\ i_g^h = \dfrac{Z_o^h}{Z_o^h + Z_g^h} i_L^h - \dfrac{1}{Z_o^h + Z_g^h} u_g^h \end{cases} \tag{1}$$

As described in (1), substantial nonlinear loads can easily contribute to serious distortion in both the output voltage u_o and grid current i_g. In addition, these power quality issues can degrade further because of the shunt circuit from the distorted grid, which results the THD of u_o and i_g much far beyond the standard level (≤5%), and poses significant challenges to the DG resilience to both critical loads and grid. It is thus appropriate to design a control scheme to suppress the individual harmonics and improve the VDG adaptability.

III. Fundamental Limitation of Simultaneous Voltage and Current Harmonic Suppression

In this section, we describe the fundamental conflict in the combined goals of harmonic voltage and current suppression. The circuit for the conventional voltage-controlled harmonic restraint scheme is shown in Fig. 4, where u_{VSG}^h is the harmonic voltage of VSG [17], [18].

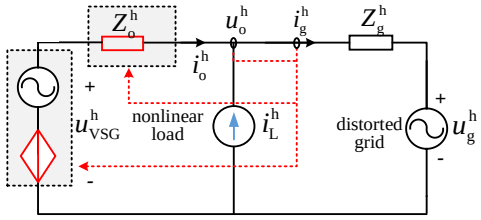

Fig. 4. Conventional harmonics suppression for voltage controlled-inverter

Then, the modified expression for u_o^h and i_g^h from Fig. 4 is given by:

$$\begin{cases} u_o^h = \dfrac{Z_g^h}{Z_o^h + Z_g^h} u_{VSG}^h + \dfrac{Z_o^h Z_g^h}{Z_o^h + Z_g^h} i_L^h + \dfrac{Z_o^h}{Z_o^h + Z_g^h} u_g^h \\ i_g^h = \dfrac{1}{Z_o^h + Z_g^h} u_{VSG}^h + \dfrac{Z_o^h}{Z_o^h + Z_g^h} i_L^h - \dfrac{1}{Z_o^h + Z_g^h} u_g^h \end{cases} \tag{2}$$

As stated in [26], in the main harmonic frequencies, the output impedance of voltage-controlled VSG is similar to the inductive impedance of synchronous generator. Then, for the convenience of analysis, we assume the dominantly inductive characteristic for the output harmonic impedance in this paper, i.e., $Z_o^h \approx j\omega_h L_o$ with L_o and ω_h as the output inductance specific harmonic frequency. Similarly, the grid harmonic impedance can also be regarded inductive dominated as $R_g \ll \omega_h L_g$ in the main harmonic frequencies, i.e., $Z_g^h \approx j\omega_h L_g$ with R_g and L_g as the grid resistance and inductance, respectively.

Therefore, the form (2) can be rearranged into an inductance characteristic expression. It can be noted in (2) that, u_{VSG}^h is supposed to be in the same direction as u_g^h to counteract the effect of u_g^h; meanwhile, for the worst case of harmonic suppression, the phases of u_{VSG}^h and u_g^h are assumed to be 90° ahead of that of i_L^h here, as shown in Fig. 5(a) with the corresponding vector diagram in Fig. 5(b).

Based on Fig. 5, it can yield,

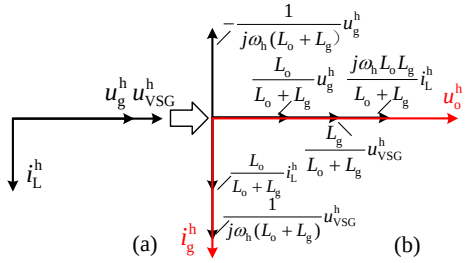

Fig. 5. Vector diagram of u_o^h and i_g^h for harmonic analysis

$$\begin{cases} U_o^h = \dfrac{L_g}{L_o + L_g} U_{VSG}^h + \dfrac{\omega_h L_o L_g}{L_o + L_g} I_L^h + \dfrac{L_o}{L_o + L_g} U_g^h \\ I_g^h = \dfrac{1}{\omega_h (L_o + L_g)} U_{VSG}^h + \dfrac{L_o}{L_o + L_g} I_L^h - \dfrac{1}{\omega_h (L_o + L_g)} U_g^h \end{cases} \tag{3}$$

where U_o^h, U_{VSG}^h, U_g^h, I_g^h and I_L^h are the effective values of u_o^h, u_{VSG}^h, u_g^h, i_g^h and i_L^h, respectively.

Further, the THD of each harmonic component at the specific distorted grid and nonlinear load can be deduced as

$$\begin{cases} \text{THD of } u_o^h(Z_o^h, u_{VSG}^h)\big|_{u_g^h=\text{constant}, i_L^h=\text{constant}} \\ \quad = \dfrac{\left| \dfrac{L_g}{L_o + L_g} U_{VSG}^h + \dfrac{\omega_h L_o L_g}{L_o + L_g} I_L^h + \dfrac{L_o}{L_o + L_g} U_g^h \right|}{U_n} \times 100\% \\ \text{THD of } i_g^h(Z_o^h, u_{VSG}^h)\big|_{u_g^h=\text{constant}, i_L^h=\text{constant}} \\ \quad = \dfrac{\left| \dfrac{1}{\omega_h (L_o + L_g)} U_{VSG}^h + \dfrac{L_o}{L_o + L_g} I_L^h - \dfrac{1}{\omega_h (L_o + L_g)} U_g^h \right|}{I_n} \times 100\% \end{cases} \tag{4}$$

Considering that an agreement for the regulation of voltage reference and output impedance can be reached from control effect perspective [19], the feasible ranges of U_{VSG}^h or Z_o^h to meet the standard requirements for u_o^h and i_g^h are calculated upon the specific case u_g^h = 5%U_n, i_L^h=5%I_n with results shown in Fig. 6.

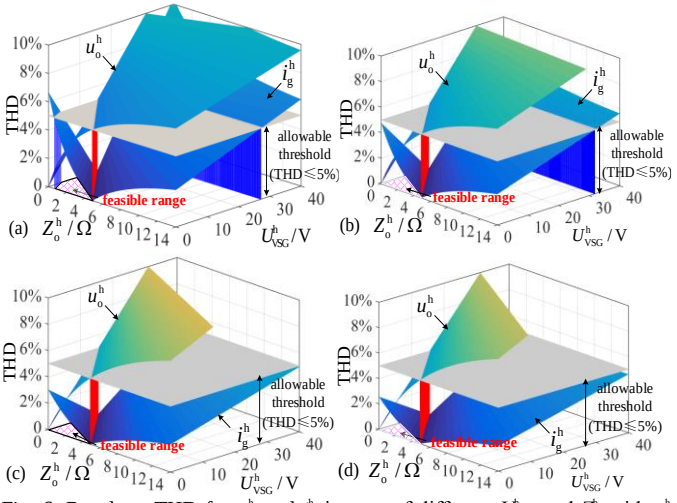

Fig. 6. Resultant THD for u_o^h and i_g^h in case of different U_{VSG}^h and Z_o^h with u_g^h =5%U_n, i_L^h=5%I_n, L_g=2.3 mH. (a) h=5. (b) h=7. (c) h=11. (d) h=13.

In this case, we assume the standard index THD of u_o and i_g ≤5% to be the specific requirement. It can be observed from Fig. 6 that the multiple hypersurfaces are generated and entrapped within an irregular domain described in (Z_o^h, U_{VSG}^h) space. The red grids at the bottom reveal the correspondences of <Z_o^h, U_{VSG}^h, u_o^h, i_g^h > to satisfy the power quality requirements for local voltage and grid current simultaneously.

This article has been accepted for publication in a future issue of this journal, but has not been fully edited. Content may change prior to final publication. Citation information: DOI 10.1109/TEC.2021.3063607, IEEE Transactions on Energy Conversion

If the system distortion gets more serious, the feasible range mentioned previously would shrink further until it disappears. Take the 5th harmonic component as an example, the feasible ranges with regard to two different sets of u_g^h and i_L^h are derived as shown in Fig. 7. With both u_g^h and i_L^h increased to 10% of their respective nominal values in Fig. 7(b), the feasible range (Z_o^h, U_{VSG}^h) that satisfies the standard constraint for both voltage and current THD are defined by A and B in red lines and blue lines, respectively. Compared to the feasible range shown in Fig. 7(a) with u_g^h(resp. i_L^h) as 5% of U_n(resp. I_n) specified from Fig. 6(a), no overlapping exists between the two parts, indicating that the harmonic voltage and harmonic current cannot be restrained simultaneously using the conventional control scheme in this case.

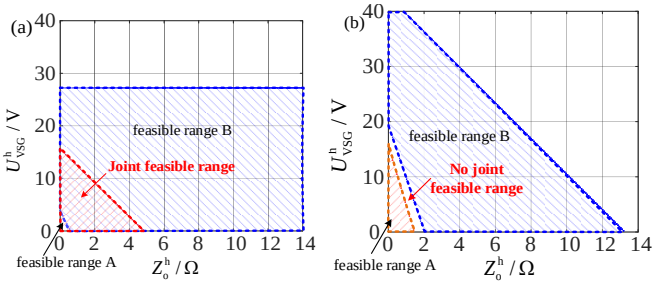

Fig. 7. Feasible ranges of U_{VSG}^h and Z_o for two sets of u_g^h, i_L^h. (a) u_g^h =5%U_n, i_L^h =5%I_n. (b) u_g^h =10%U_n, i_L^h=10%I_n.

From the analysis above, the two feasible ranges shift in the opposite directions, thus revealing analytically that nonlinear load current and distorted grid voltage are two constrained harmonic sources. From the viewpoint of control principle, the desired scheme is described as: 1) the output impedance Z_o^h is expected to be small and then most of nonlinear load currents can be absorbed by VSG side; 2) the local voltage distortion is supposed to be reduced as much as possible for critical loads; 3) grid current distortion is reduced greatly, which indicates a large harmonic impedance from grid to load point. A proper control scheme is indispensable to address both harmonic local voltage and grid current to improve VSG power quality.

IV. Proposed Control Scheme For VSG Harmonic Voltage and Grid Current Suppression

A. Adaptive Multiple-Harmonic Observer

Obviously, a linear circuit with various frequencies can be analyzed separately at each frequency based on superposition theorem, which is used to address this issue. Because accurate harmonic detection is of major significance, an MHSCO is introduced in this paper to extract the individual harmonic sequences instead of the conventional low pass filter (LPF). The estimator assigned for the *h*-th harmonic component can be formulized [27]

$$\hat{x}_{k+1}^h = e^{jh\omega T_s}\hat{x}_k^h + \frac{\omega_c T_s}{1+n\omega_c T_s}(v_k - \sum_m e^{jm\omega T_s}\hat{x}_k^{(m)}) \quad (5)$$

where v_k is the input signal before the filtering process and it is harmonic current or voltage in this paper; $\hat{x}_{k+1}^h$ is the estimate of the *h*-th harmonic of current or voltage under study; ω_c is the cut-off frequency of the observer; T_s is the sampling period; m is the number of the major harmonics estimated.

Compared to the conventional LPF harmonic extraction approach, the MHSCO algorithm takes the advantage of adaptive state observer which not only facilitates the superior dynamics and accuracy for the multi-order harmonic estimation but also reduces the computational burden at the exhaustive frequencies. With ζ as the damping ration, the transfer function of MHSCO can be reduced as [27]

$$G_{MHSCO}^h(s) = \frac{\zeta\omega_h s}{(1+\sum_{l=1,-5,+7,\ldots}^{l\neq h}\frac{\zeta\omega_l s}{s^2+\omega_l^2})(s^2+\omega_h^2)+\zeta\omega_h s} \quad (6)$$

We use the extraction of the 5th harmonic as an example, and the frequency response characteristics obtained from both of MHSCO and LPF methods are depicted in Fig. 8 with the same ζ of 0.707. It can be observed that the magnitudes of MHSCO and LPF at the 5th harmonic frequency is 0 dB, which indicates that both methods can maintain the amplitude at the concerned frequency without any attenuation. Whereas, compared with LPF, the magnitude notches in MHSCO at the fundamental, 7th, 11th, 13th harmonic frequencies are attenuated substantially, which indicates that these undesired harmonic orders are subtracted through MHSCO when estimating the 5th harmonic component. The result shows that the proposed approach enables the more accurate and exhaustive extraction for the individual frequencies we interest, which facilities the effective harmonic suppression for VSG.

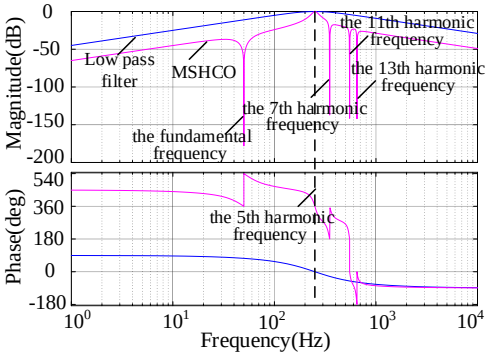

Fig. 8. Comparison of frequency responses of MHSCO and LPF for the extraction of 5th harmonic.

B. Harmonic Suppression Scheme With Tunable Tradeoff

Based on the intrinsic contradiction of suppressing the two distortions entirely using one control variable, a control scheme with a tunable tradeoff between voltage and current distortions is presented in Fig. 9, additional to fundamental VSG scheme.

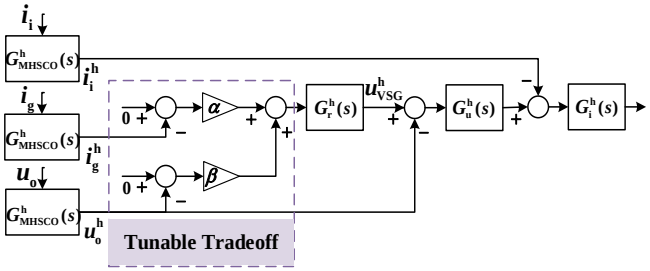

Fig. 9. Structure of unified harmonic suppression with a tunable tradeoff.

As shown in Fig. 9, the VSG harmonic voltage reference is

$$u_{VSG}^h = G_r^h(s)[\alpha(0-i_g^h)+\beta(u_o^h-0)] \quad (7)$$

where $G_r^h(s)$ is PI controller; α and β are two positive bias factors; a dual loop is used to track u_{VSG}^h with $G_u^h(s)$ as PI controller and $G_i^h(s)$ as P controller. When the system is stable,

This article has been accepted for publication in a future issue of this journal, but has not been fully edited. Content may change prior to final publication. Citation information: DOI 10.1109/TEC.2021.3063607, IEEE Transactions on Energy Conversion

we can obtain

$$\alpha(0-i_g^h)+\beta(u_o^h-0)=0 \tag{8}$$

Combining (1) with (6), it yields

$$Z_o^h=\frac{\alpha u_g^h}{\alpha i_L^h+\beta(u_g^h+Z_g^h i_L^h)} \tag{9}$$

The controller (7) achieves a tunable compromise between the power qualities of the local voltage and grid current. We consider the three cases as follows.

Case 1 ($\alpha = 0, \beta \neq 0$): The first term in (8) disappears, leaving only the second term for local voltage distortion suppression. The steady state requires the harmonic voltage u_o^h to be zero and the harmonic grid current i_g^h to be the constant value $-u_g^h/Z_g^h$.

Case 2 ($\alpha \neq 0$, $\beta = 0$): In contrast to Case 1, the absence of second term in (8) indicates that the controller stresses purely on the suppression of grid distortion, which implies that the harmonic output voltage u_o^h equals to the grid voltage u_g^h.

Case 3 ($\alpha \neq 0, \beta \neq 0$): In this case, a compromise between the two goals mentioned above can be achieved upon the specific variables α and β. If the THD of i_g is higher than the threshold, a bigger α is then preferable. However, if the power quality of critical loads must be guaranteed first, the factor β can be weighted more heavily than α.

It is worth noting that this tunable tradeoff-based unified control scheme is appropriate for a single or loosely control goal, i.e., for the voltage or current harmonic, or combined inhibition in case of slight system distortion. For the more stringent objective or for serious distortions, a complete harmonic suppression scheme based on adaptive voltage compensation is proposed hereafter.

C. Complete Harmonic Suppression Scheme

Fig. 10 shows the principle of proposed control scheme for suppressing the distortions of local voltage and grid current simultaneously, which is mainly consists of the local voltage feedback loop and the grid current-controlled loop.

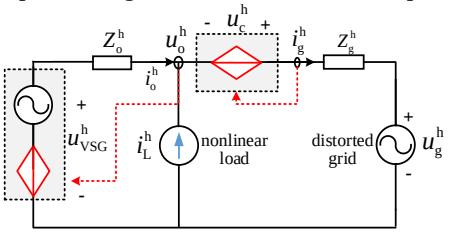

Fig. 10. Equivalent circuit with the proposed harmonic suppression method

The expression for (1) can then be modified as shown:

$$\begin{cases} u_o^h=\dfrac{Z_g^h}{Z_o^h+Z_g^h}u_{VSG}^h+\dfrac{Z_o^h Z_g^h}{Z_o^h+Z_g^h}i_L^h+\dfrac{Z_o^h}{Z_o^h+Z_g^h}(u_g^h-u_c^h) \\ i_g^h=\dfrac{1}{Z_o^h+Z_g^h}u_{VSG}^h+\dfrac{Z_o^h}{Z_o^h+Z_g^h}i_L^h-\dfrac{1}{Z_o^h+Z_g^h}(u_g^h-u_c^h) \end{cases} \tag{10}$$

Theoretically, as depicted in (10), the adverse effects of i_L^h on i_g^h and u_o^h could be eliminated when $u_{VSG}^h+Z_o^h i_L^h=0$, meaning that the terms $Z_g^h u_{VSG}^h/(Z_o^h+Z_g^h)+Z_o^h Z_g^h i_L^h/(Z_o^h+Z_g^h)$ and $u_{VSG}^h/(Z_o^h+Z_g^h)+Z_o^h i_L^h/(Z_o^h+Z_g^h)$ can be cancelled in this case. Additionally, the effect of grid harmonic u_g^h on i_g^h and u_o^h could be resisted efficiently when the accessional voltage set u_c^h is equal to u_g^h; this can be obtained by introducing a current-controlled voltage between the local bus and the grid side, as shown in Fig. 10.

The proposed control scheme is implemented as depicted in Fig. 11. The harmonic components u_o^h and i_i^h are extracted through the MHSCO firstly. The fundamental voltage reference and harmonic voltage reference are generated by the conventional VSG control and harmonic voltage control loop respectively, total of which are fed into the cascade voltage and current control as the VSG voltage reference u_{VSG}^*. Then the

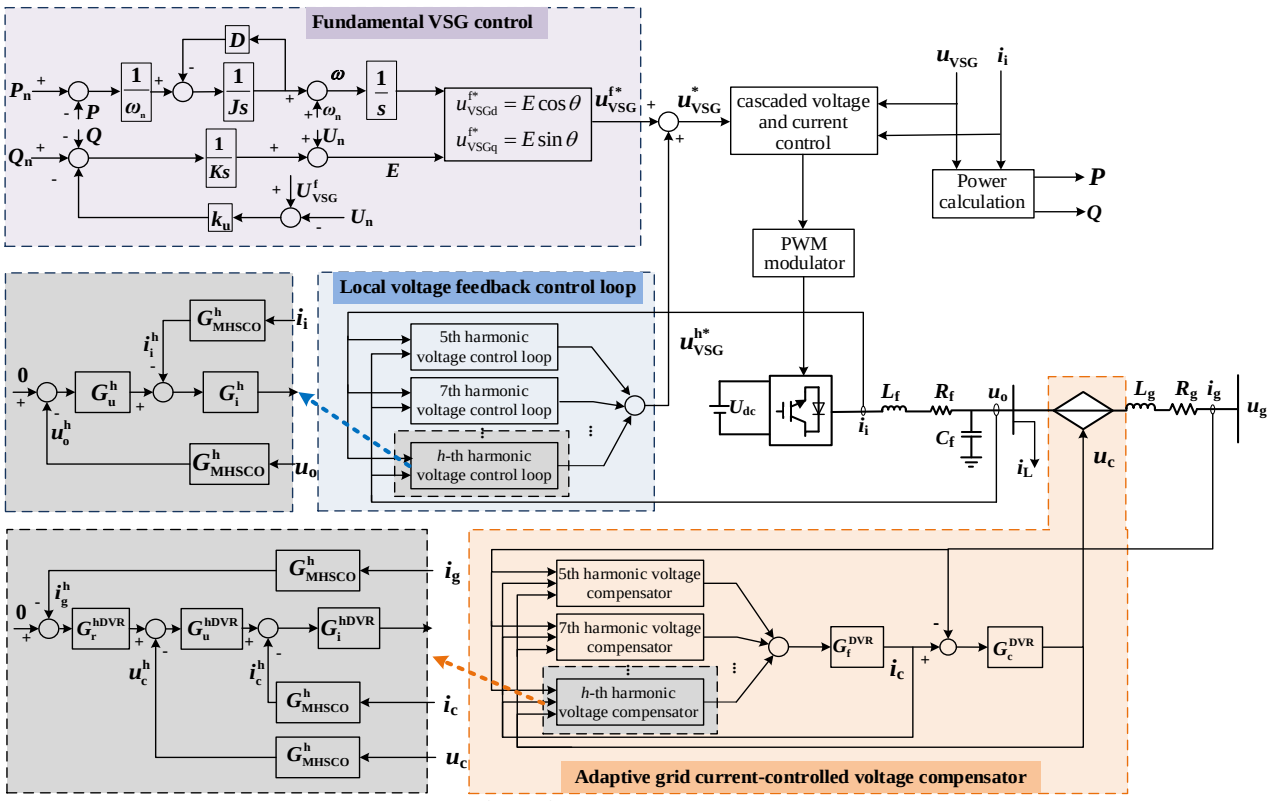

Fig. 11 Control scheme structure for the fundamental dynamics and complete harmonic suppression

This article has been accepted for publication in a future issue of this journal, but has not been fully edited. Content may change prior to final publication. Citation information: DOI 10.1109/TEC.2021.3063607, IEEE Transactions on Energy Conversion

harmonic voltage that is dropped on the inverter output impedance can be compensated. Additionally, an adaptive grid current-controlled compensator is designed to counteract the adverse effects of distorted grid. The two harmonic control loops are elaborated in the following.

With the proposed harmonic voltage control, the closed-loop transfer function of output voltage/current (equivalent output impedance viewed from PCC to VSG) is described as:

$$Z_{\mathrm{o}}=\frac{u_{\mathrm{o}}}{i_{\mathrm{o}}}=\frac{k_{\mathrm{pwm}}^{\mathrm{h}}G_{\mathrm{f}}G_{\mathrm{c}}(G_{\mathrm{Mi}}+G_{\mathrm{i}}^{\mathrm{h}})+G_{\mathrm{c}}}{k_{\mathrm{pwm}}^{\mathrm{h}}G_{\mathrm{f}}(G_{\mathrm{u}}^{\mathrm{h}}G_{\mathrm{i}}^{\mathrm{h}}G_{\mathrm{c}}+G_{\mathrm{c}}G_{\mathrm{Mui}}+G_{\mathrm{Mi}}+G_{\mathrm{i}}^{\mathrm{h}})+1} \tag{11}$$

where $k_{\mathrm{pwm}}^{\mathrm{h}}$ is the inverter voltage gain; G_f and G_c are the inductance and capacitance branches of LC filter. $G_{\mathrm{u}}^{\mathrm{h}}=k_{\mathrm{pu}}^{\mathrm{h}}+k_{\mathrm{iu}}^{\mathrm{h}}/\mathrm{s}$ and $G_{\mathrm{i}}^{\mathrm{h}}=k_{\mathrm{pi}}^{\mathrm{h}}$ with $k_{\mathrm{pu}}^{\mathrm{h}}$, $k_{\mathrm{pi}}^{\mathrm{h}}$ proportional gains and $k_{\mathrm{iu}}^{\mathrm{h}}$ integral gain.

$$G_{\mathrm{Mi}}=\sum_{m=1,2,\ldots}G_{\mathrm{MHSCO}}^{(6m\pm1)}G_{\mathrm{i}}^{(6m\pm1)},\quad G_{\mathrm{Mui}}=\sum_{m=1,2,\ldots}G_{\mathrm{MHSCO}}^{(6m\pm1)}G_{\mathrm{u}}^{(6m\pm1)}G_{\mathrm{i}}^{(6m\pm1)}$$

To demonstrate the effect of the proposed method, Bode plots of total $Z_{\mathrm{o}}(s)$ with and without the voltage feedback control loop are shown in Fig. 12, from which we observe that the VSG output impedance Z_{o} is greatly scaled down at the h-th harmonic when compared with the original value, which results in a smaller harmonic voltage drop on the output impedance. Then, most of the load harmonic current $i_{\mathrm{L}}^{\mathrm{h}}$ would flow into the VSG side rather than grid side due to the reduced equivalent output impedance, conducive to the improvement of the local voltage quality. It is noteworthy that the harmonic current introducing from nonlinear load is expected to be absorbed by the remaining harmonic capacity of VSG, which is subject to the specific rating and fundamental output power of VSG. If the nonlinear load is smaller than the VSG remaining capacity, nonlinear harmonic currents would be suppressed effectively by VSG; otherwise, besides the substantial harmonics absorbed by VSG, the counterpart flowing into the grid can be retrained by an additional voltage compensator, introduced hereafter.

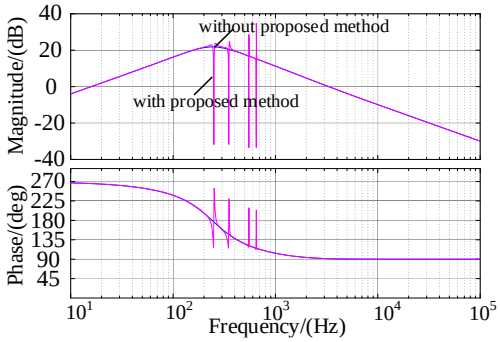

Fig. 12. Bode plot of Z_{o} with and without the proposed method

Considering the distorted grid current caused by the grid harmonic voltage $u_{\mathrm{g}}^{\mathrm{h}}$, an adaptive grid current-controlled voltage is introduced as shown in Fig. 11 to generate the additional compensation u_{c} to eliminate the effects of distorted grid voltage. Based on the condition that the VSG output voltage harmonics have been canceled fully with the previous local voltage control step, i.e., $u_{\mathrm{o}}^{\mathrm{h}}=0$, the dynamics of grid current in a synchronous rotating frame can be expressed as:

$$\begin{cases}L_{\mathrm{g}}\dfrac{di_{\mathrm{cd}}^{\mathrm{h}}}{dt}=u_{\mathrm{cd}}^{\mathrm{h}}-R_{\mathrm{g}}i_{\mathrm{cd}}^{\mathrm{h}}+\omega_{\mathrm{h}}L_{\mathrm{g}}i_{\mathrm{cq}}^{\mathrm{h}}-u_{\mathrm{gd}}^{\mathrm{h}}\\ L_{\mathrm{g}}\dfrac{di_{\mathrm{cq}}^{\mathrm{h}}}{dt}=u_{\mathrm{cd}}^{\mathrm{h}}-R_{\mathrm{g}}i_{\mathrm{cq}}^{\mathrm{h}}-\omega_{\mathrm{h}}L_{\mathrm{g}}i_{\mathrm{cd}}^{\mathrm{h}}-u_{\mathrm{gq}}^{\mathrm{h}}\end{cases} \tag{12}$$

where $u_{\mathrm{cd}}^{\mathrm{h}}$, $u_{\mathrm{cq}}^{\mathrm{h}}$, $u_{\mathrm{gd}}^{\mathrm{h}}$, $u_{\mathrm{gq}}^{\mathrm{h}}$ $i_{\mathrm{cd}}^{\mathrm{h}}$, and $i_{\mathrm{cq}}^{\mathrm{h}}$ are $u_{\mathrm{c}}^{\mathrm{h}}$, $u_{\mathrm{g}}^{\mathrm{h}}$ and $i_{\mathrm{c}}^{\mathrm{h}}$ in d and q axes, respectively; if $u_{\mathrm{cd}}^{\mathrm{h}}=u_{\mathrm{gd}}^{\mathrm{h}}$ and $u_{\mathrm{cq}}^{\mathrm{h}}=u_{\mathrm{gq}}^{\mathrm{h}}$, we can get $i_{\mathrm{cd}}^{\mathrm{h}}=i_{\mathrm{cq}}^{\mathrm{h}}=0$. Considering the normally inductive domain characteristics of the grid impedance, the harmonic current controller yields

$$\begin{cases}u_{\mathrm{cd}}^{\mathrm{h}*}=-G_{\mathrm{r}}^{\mathrm{hDVR}}(0-i_{\mathrm{cq}}^{\mathrm{h}})\\ u_{\mathrm{cq}}^{\mathrm{h}*}=G_{\mathrm{r}}^{\mathrm{hDVR}}(0-i_{\mathrm{cd}}^{\mathrm{h}})\end{cases} \tag{13}$$

where $u_{\mathrm{cd}}^{\mathrm{h}*}$ and $u_{\mathrm{cq}}^{\mathrm{h}*}$ are the reference values for harmonic voltage compensation in d and q axes; $G_{\mathrm{r}}^{\mathrm{hDVR}}=(k_{\mathrm{pr}}^{\mathrm{hDVR}}+k_{\mathrm{ir}}^{\mathrm{hDVR}}/\mathrm{s})$ with the proportional gain $k_{\mathrm{pr}}^{\mathrm{hDVR}}$ and the integral gain $k_{\mathrm{ir}}^{\mathrm{hDVR}}$.

A conventional cascaded voltage and current controller is then used to track the voltage harmonic references. The transfer function of the grid voltage to grid current can be deduced as (14), where $k_{\mathrm{pwm}}^{\mathrm{hDVR}}$ is the voltage gain; $G_{\mathrm{f}}^{\mathrm{DVR}}$ and $G_{\mathrm{c}}^{\mathrm{DVR}}$ are the inductance and capacitance branches of LC filter in the current-controlled voltage compensator; $G_{\mathrm{u}}^{\mathrm{hDVR}}=k_{\mathrm{pu}}^{\mathrm{hDVR}}+k_{\mathrm{iu}}^{\mathrm{hDVR}}/\mathrm{s}$ and $G_{\mathrm{i}}^{\mathrm{hDVR}}=k_{\mathrm{pi}}^{\mathrm{hDVR}}$ are the PI and P controllers; G_{g} is the grid impedance.

$$G_{\mathrm{Mrui}}^{\mathrm{DVR}}=\sum_{m=1,2,\ldots}G_{\mathrm{MHSCO}}^{(6m\pm1)}G_{\mathrm{i}}^{(6m\pm1)\mathrm{DVR}}[1+G_{\mathrm{r}}^{(6m\pm1)\mathrm{DVR}}G_{\mathrm{u}}^{(6m\pm1)\mathrm{DVR}}]$$

$$G_{\mathrm{Mui}}^{\mathrm{DVR}}=\sum_{m=1,2,\ldots}G_{\mathrm{MHSCO}}^{(6m\pm1)}G_{\mathrm{u}}^{(6m\pm1)\mathrm{DVR}}G_{\mathrm{i}}^{(6m\pm1)\mathrm{DVR}}$$

A comparison of the Bode plots of equivalent grid admittance $Y_{\mathrm{g}}(s)$ with and without the proposed method is presented in Fig. 13 to illustrate the effects of the adaptive current-controlled voltage compensator. The plots show that the admittance amplitudes at the harmonic frequencies of interest are attenuated substantially with the proposed method, which implies that the harmonic current caused by the distortion grid voltage $u_{\mathrm{g}}^{\mathrm{h}}$ would be suppressed effectively.

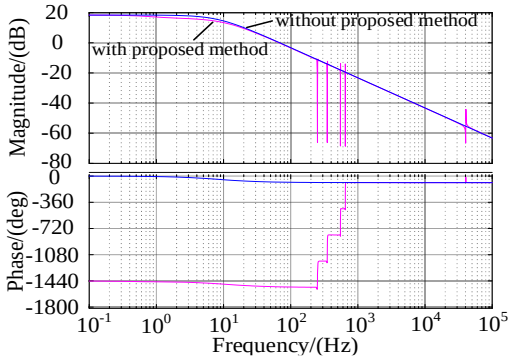

Fig. 13. Bode plots of Y_{g} with and without the proposed method

Therefore, the distortions of local voltage and grid current are addressed by modifying the equivalent output impedance Z_{o} and the grid admittance Y_{g}, respectively. The power quality of VSG could evidently be improved at the same time, regardless of the variations in $u_{\mathrm{g}}^{\mathrm{h}}$, $i_{\mathrm{L}}^{\mathrm{h}}$ and $Z_{\mathrm{g}}^{\mathrm{h}}$. It should be noted that based on the superposition theorem, the fundamental dynamics mainly depend on the conventional VSG control, and harmonic suppression is decided by the proposed control scheme, with multiple circuits designated and implemented independently.

$$Y_{\mathrm{g}}(s)=\frac{i_{\mathrm{g}}}{u_{\mathrm{g}}}=\frac{G_{\mathrm{g}}(k_{\mathrm{pwm}}^{\mathrm{hDVR}}G_{\mathrm{f}}^{\mathrm{DVR}}(G_{\mathrm{u}}^{\mathrm{hDVR}}G_{\mathrm{i}}^{\mathrm{hDVR}}G_{\mathrm{c}}^{\mathrm{DVR}}+G_{\mathrm{c}}^{\mathrm{DVR}}G_{\mathrm{Mui}}+G_{\mathrm{Mrui}}+G_{\mathrm{i}}^{\mathrm{DVR}})+G_{\mathrm{f}}^{\mathrm{DVR}}G_{\mathrm{c}}^{\mathrm{DVR}}+1)}{k_{\mathrm{pwm}}^{\mathrm{hDVR}}G_{\mathrm{f}}^{\mathrm{DVR}}(G_{\mathrm{u}}^{\mathrm{hDVR}}G_{\mathrm{i}}^{\mathrm{hDVR}}G_{\mathrm{c}}^{\mathrm{hDVR}}+G_{\mathrm{i}}^{\mathrm{hDVR}}G_{\mathrm{c}}^{\mathrm{DVR}}G_{\mathrm{g}}+G_{\mathrm{c}}^{\mathrm{DVR}}G_{\mathrm{g}}G_{\mathrm{Mrui}}+G_{\mathrm{c}}^{\mathrm{DVR}}G_{\mathrm{Mui}}+G_{\mathrm{Mrui}}+G_{\mathrm{i}}^{\mathrm{hDVR}})+G_{\mathrm{f}}^{\mathrm{DVR}}G_{\mathrm{c}}^{\mathrm{DVR}}+G_{\mathrm{c}}^{\mathrm{DVR}}G_{\mathrm{g}}+1} \tag{14}$$

This article has been accepted for publication in a future issue of this journal, but has not been fully edited. Content may change prior to final publication. Citation information: DOI 10.1109/TEC.2021.3063607, IEEE Transactions on Energy Conversion

Therefore, besides the fundamental VSG performance, the individual harmonic components can be diminished effectively.

D. Small-Signal Model and Stability Analysis

The stability analysis of the tunable tradeoff-based controller (7) is easy to track and is beyond the scope of this paper. In this Section, we present a small-signal analysis of the complete harmonic suppression scheme, through which the potential effects of parameter perturbation can be investigated. The system small-signal model is established subsequently using three parts: the inverter, the network and the controller.

First, the inverter at the *h*-th harmonic frequency in dq frame with the proposed harmonic voltage control can be expressed as

$$\begin{cases} L_o \dfrac{di_{od}^h}{dt} = u_{VSGd}^h - R_o i_{od}^h + \omega_h L_o i_{oq}^h - u_{od}^h \\ L_o \dfrac{di_{oq}^h}{dt} = u_{VSGq}^h - R_o i_{oq}^h - \omega_h L_o i_{od}^h - u_{oq}^h \end{cases} \tag{15}$$

where i_{od}^h and i_{oq}^h (resp. u_{od}^h and u_{oq}^h) are the output harmonic current (resp. voltage) along the d and q axes, respectively; R_o and L_o are the equivalent output resistance and inductance of VSG, respectively. Then, the voltage harmonic references u_{VSGd}^h and u_{VSGq}^h are generated as

$$\begin{bmatrix} u_{VSGd}^h \\ u_{VSGq}^h \end{bmatrix} = \begin{bmatrix} k_{ir}^h & 0 \\ 0 & k_{ir}^h \end{bmatrix} \begin{bmatrix} x_d \\ x_q \end{bmatrix} + \begin{bmatrix} k_{pr}^h & 0 \\ 0 & k_{pr}^h \end{bmatrix} \begin{bmatrix} 0-u_{od}^h \\ 0-u_{oq}^h \end{bmatrix}$$
$$\begin{bmatrix} \dot{x}_d \\ \dot{x}_q \end{bmatrix} = \begin{bmatrix} 0-u_{od}^h \\ 0-u_{oq}^h \end{bmatrix} \tag{16}$$

where x_d and x_q denote the auxiliary states from PI controller along d and q axes, with k_{pr}^h and k_{ir}^h as the proportional and integral gains. The additional voltage source u_{cd}^h and u_{cq}^h are calculated as follows:

$$\begin{bmatrix} u_{cd}^h \\ u_{cq}^h \end{bmatrix} = \begin{bmatrix} -k_{ir}^{hDVR} & 0 \\ 0 & k_{ir}^{hDVR} \end{bmatrix} \begin{bmatrix} x_d^{DVR} \\ x_q^{DVR} \end{bmatrix} + \begin{bmatrix} -k_{pr}^{hDVR} & 0 \\ 0 & k_{pr}^{hDVR} \end{bmatrix} \begin{bmatrix} 0-i_{gq}^h \\ 0-i_{gd}^h \end{bmatrix}$$
$$\begin{bmatrix} \dot{x}_d^{DVR} \\ \dot{x}_q^{DVR} \end{bmatrix} = \begin{bmatrix} 0-i_{gq}^h \\ 0-i_{gd}^h \end{bmatrix} \tag{17}$$

where x_d^{DVR} and x_q^{DVR} are the auxiliary states from PI controller along d and q axes, with k_{pr}^{hDVR} and k_{ir}^{hDVR} as the proportional and integral gains. It should be noted that due to the dominant inductance of grid impedance Z_g, the variables in d and q axes of u_c^h correspond to those of q and d axes of i_g^h, respectively. The dynamics of grid connection current can also be obtained as

$$\begin{cases} L_g \dfrac{di_{gd}^h}{dt} = u_{od}^h + u_{cd}^h - R_g i_{gd}^h + \omega_h L_g i_{gq}^h - u_{gd}^h \\ L_g \dfrac{di_{gq}^h}{dt} = u_{oq}^h + u_{cq}^h - R_g i_{gq}^h - \omega_h L_g i_{gd}^h - u_{gq}^h \end{cases} \tag{18}$$

where i_{gd}^h and i_{gq}^h are the grid harmonic current i_g^h along the d and q axes. By linearizing and combining (15)-(18), the small-signal model of the overall system can be formulated as

$$\dot{\boldsymbol{x}} = \boldsymbol{A}\boldsymbol{x} \tag{19}$$

where $\boldsymbol{x} = [i_{od}^h, i_{oq}^h, x_d, x_q, i_{gd}^h, i_{gq}^h, x_d^{DVR}, x_q^{DVR}]^T$; $\boldsymbol{A}$ is the state and input matrices, which can be obtained from (15)–(18).

The acquisition of system small-signal model allows the parameter perturbation on system dynamics to be investigated. Here, we use the grid impedance L_g as an example because it would vary easily with the background grid. Based on the system parameters in Table I, the resulting dynamics are elaborated with the eigenvalue locus, as depicted in Fig. 14. As shown in Fig. 14, when L_g increases, the dominant eigenvalues $\lambda_{5,6,7,8}$ tend to move further away from the imaginary axis, thus indicating better stability. However, the profile behaviors of $\lambda_{9,10}$ are opposite to those of $\lambda_{5,6,7,8}$ and gradually approach the imaginary axis under the same condition, which indicates the adaptability of proposed strategy to the perturbation of parameter L_g. In practice, L_g should be maintained to be neither too large nor too small; otherwise, the system stability would be threatened.

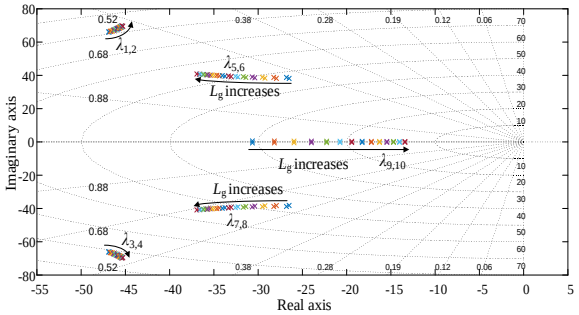

Fig. 14. Eigenvalues locus with grid impedance: 0.5mH ≤ L_g ≤3.1mH

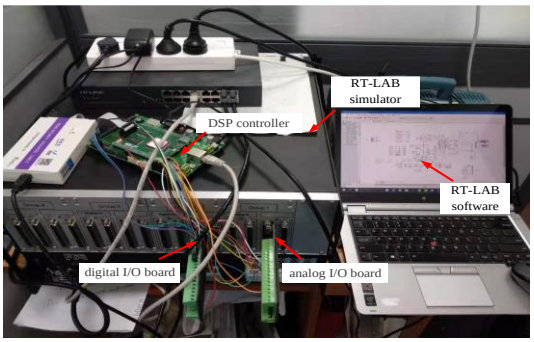

Fig. 15 HIL simulation platform based on RT-LAB

V. Simulation Evaluation

To verify the effectiveness of the proposed strategy, cases based on the VSG structure shown in Fig. 1 are studied through the controller HIL platform, as shown in Fig. 15. The main circuit is built by RT-LAB system (i.e., real-time simulator OPAL-RT) and the harmonic control algorithm is programmed using a TMS320F28377 DSP, which acquires measurements and sends control signals to the RT-LAB simulator via the digital and analog I/O boards to imitate the operation more realistically. The main circuit and control parameters are listed.

TABLE I
System and Control Parameters

System Parameter	Value	System Parameter	Value
Rating capacity S_N	30 kVA	Grid inductance L_g	2.3 mH
VSG bus voltage U_{dc}	800 V	Sampling period T_s	50 us
Filter inductance L_f	2 mH	Resistance of NL R_{nl}	25 Ω
Filter capacity C_f	50 uF	Capacitance of NL C_{nl}	400 uF
Grid resistance R_g	0.12 Ω	Inductance of NL L_{nl}	0.6 mH
Harmonic Controller		*h*=5	*h*=7
k_{pu}^h, k_{iu}^h; k_{pi}^h		1,100;20;	1,80;15;
k_{pr}^{hDVR},k_{ir}^{hDVR}; k_{pu}^{hDVR}, k_{iu}^{hDVR}; k_{pi}^{hDVR}		0.5,150;2,100;18;	0.5,100;2,100;15;

This article has been accepted for publication in a future issue of this journal, but has not been fully edited. Content may change prior to final publication. Citation information: DOI 10.1109/TEC.2021.3063607, IEEE Transactions on Energy Conversion

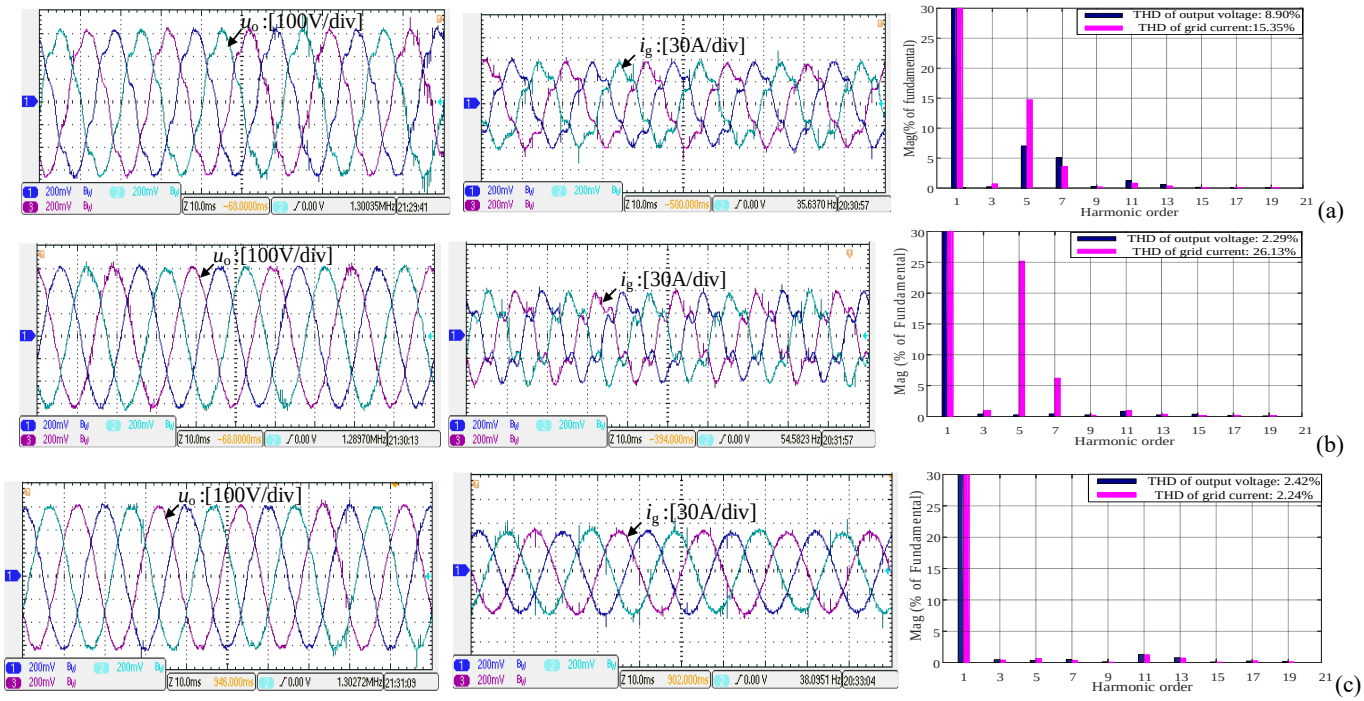

Fig. 16. Simulation results of voltage and current harmonics suppression. (a) Results without harmonic suppression. (b) Results with proposed voltage control loop only. (c)Results with proposed hybrid harmonic suppression method.

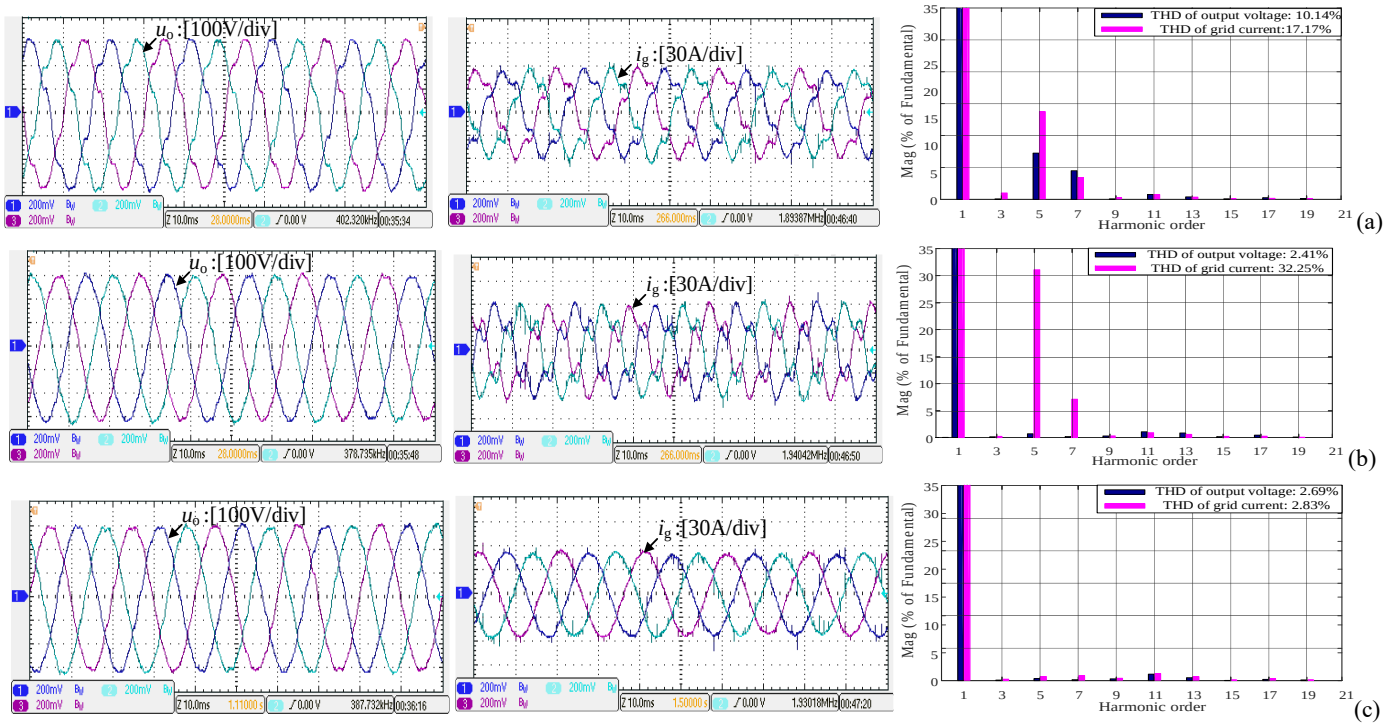

Fig. 17 Simulation results of the robustness against L_g variation. (a) Results without harmonic suppression. (b) Results with proposed voltage control loop only. (c)Results with proposed hybrid harmonic suppression method.

in Table I. In this case, it is assumed that the 5th and 7th harmonic components take over the majority of the distorted grid voltage, with magnitudes of 20% and 10% of the fundamental AC voltage. In the scenarios that follow, the simulation profiles are observed using a Tektronix MDO3020 oscilloscope.

A. Control Performance for Harmonic Suppression

In this case, the performance of the proposed harmonic suppression method is investigated. First, the voltage harmonic suppression algorithm operates at t=4 s, and the current harmonic suppression is subsequently activated at 4.5 s, with the simulation results shown in Fig. 16. It can be observed from Fig. 16(a) that the output voltage and the grid current of VSG are seriously distorted initially, with the THDs of the voltage and current being as high as 8.90% and 15.35%, respectively. After the proposed voltage control loop is introduced, a significant improvement occurs in the THD of output

This article has been accepted for publication in a future issue of this journal, but has not been fully edited. Content may change prior to final publication. Citation information: DOI 10.1109/TEC.2021.3063607, IEEE Transactions on Energy Conversion

voltage,which ranges from 8.90% to 2.29%, as shown in Fig. 16(b), with power quality improvement by 74.3%. However, the THD of grid current increases notably from 15.35% to 26.13%, due to the contradiction between the voltage and current harmonics suppression mentioned previously in Section III. When the proposed adaptive grid current-controlled compensator is started at 4.5 s, the THD of grid current is reduced from 26.13% to 2.24%, while the THD of output voltage is maintained as low as 2.42% as shown in Fig. 16(c). In theory, the THDs of both output voltage and grid current could be reduced to zero using the proposed hybrid harmonic suppression method; however, only the 5th and 7th harmonic voltage and current controllers are implemented in this paper rather than including their counterparts for all harmonic frequencies, considering the predominant harmonic orders in this case. Meanwhile, the 11th and 13th harmonic components increase slightly because of the changes in the voltage or current profiles caused by the reduction of the 5th and 7th harmonics. Therefore, the effectiveness of the proposed strategy in dealing with the harmonics of both output voltage and grid current simultaneously is validated.

B. Performance With Regard to Parameter Variation

To evaluate the robustness of proposed method to L_g variation, simulations are performed with the results obtained shown in Fig. 17 when L_g decreased from 2.3 mH to 1.8 mH. Comparison of the responses in Fig. 16(a) and Fig. 17(a) shows that the THDs of the output voltage and grid current increase slightly from 8.90% to 10.14%, and from 15.35% to 17.17% respectively without harmonic suppression, because of the reduction in L_g. When the proposed voltage control is utilized, the output voltage THD drops to 2.41% in Fig. 17(b), which is quite close to that in Fig. 16(b). However, the grid current deteriorates more seriously with THD of 32.25%. After the grid current-controlled compensator functions, the THDs of output voltage and grid current are maintained at 2.69% and 2.83% respectively, slightly higher than those in Fig. 16(c), but far lower than the standard level 5%, indicating that the proposed strategy is robust against the variation in the grid impedance.

C. Robustness to Load Variation

An additional simulation is performed to evaluate the effectiveness of the proposed strategy in the presence of load fluctuations. A resistive load 10 kW is suddenly connected to the inverter at t=5 s and disconnected at t=5.3 s. At t=5.5 s, the nonlinear load is twice as much as that in Case A. The corresponding simulation results are shown in Fig. 18(b) and 18(c), from which it can be seen that the harmonics of output voltage and grid current are both suppressed effectively with THDs 1.92% and 3.19% (resp. 2.02% and 3.4%), respectively, which indicates the robustness of the proposed strategy against both linear and nonlinear load variations. Additionally, due to the improved local voltage, the distortion of linear load current we interest is only 1.26% (as depicted in Fig. 18(d)) and then the power quality for linear critical loads can be guaranteed regardless of the distorted grid and nonlinear loads.

To verify the advantage of the proposed method, a comparison to the harmonic suppression method [26] is implemented with the same operation aforementioned, and the simulation results are shown in Fig. 19. It can be observed that with impedance-based harmonic suppression, both the distortion of inverter voltage and grid current can be suppressed within 3.08% and 2.88%, respectively. However, with the connection of additional linear and nonlinear loads, the THD of grid current increases from 2.88% to 6.3%; this is mainly because the harmonic current flowing into the grid is proportional to the nonlinear load, consist with the result in Section V of [26], whereas the THD of local voltage slightly increases to 3.65% due to the relatively small harmonic voltage drop across the grid impedance. Then, the superiority of proposed scheme to the comparison method in dealing with load variation is demonstrated.

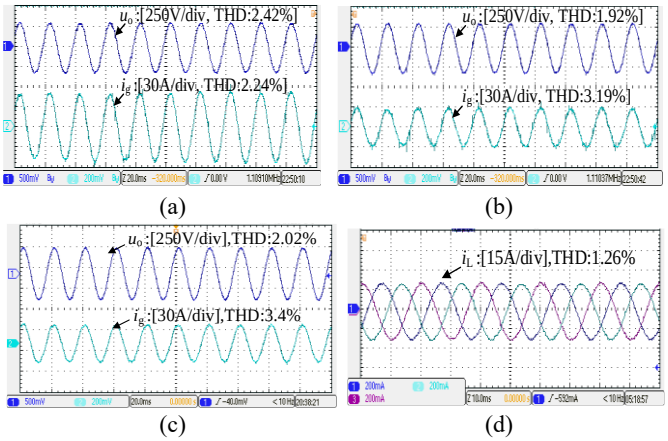

Fig. 18 Simulation results of the robustness to load variation of the proposed method. (a) Before load increases. (b) With increased linear load. (c) With increased nonlinear load. (d) Linear load current.

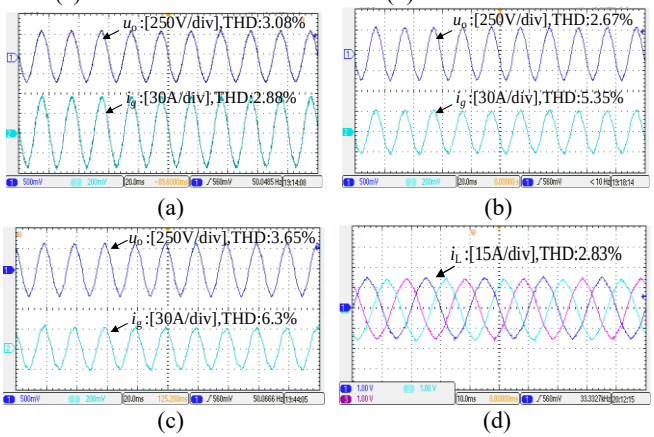

Fig. 19 Simulation results of the robustness to load variation of the comparison method. (a) Before load increases. (b) With increased linear load. (c) With increased nonlinear load. (d) Linear load current.

VI. CONCLUSION

In view of the inherent contradiction involved in attenuating adverse effects in the presence of nonlinear loads and distorted grid, this paper presents tunable tradeoff between constrained harmonic sources. A hybrid harmonic suppression scheme is then proposed and consists of a local voltage harmonic control loop and an adaptive grid current-controlled loop, with a concurrent distortion inhibition capability. Compared with the existing approaches, the proposed methodology provides high-quality power supplies for both the grid and local loads.

REFERENCES

[1] Q. Zhong, and G. Weiss, "Synchronverters: inverters that mimic synchronous generators," *IEEE Trans. Ind. Electron.*, vol. 58, no. 4, pp. 1259-1267, Apr. 2011.

[2] J. Ailpoor, Y. Miura, and T. Ise, "Power system stabilization using virtual synchronous generator with alternating moment of inertia," *IEEE Journal Emerg. Sel. Topics Power Electron.*, vol. 3, no. 2, pp. 451-458, June 2014.

[3] J. Liu, Y. Miura, and T. Ise, "Comparison of dynamic characteristics between virtual synchronous generator and droop control in inverter-based distributed generators," *IEEE Trans. Power Electron.*, vol. 31, no. 5, pp. 3600-3611, May 2016.

[4] D. Arricibita, P. Sanchis, and L. Marroyo, "Virtual synchronous generators classification and common trends", in *Proc. IECON*, 2016, pp. 2433-2438.

[5] J. Fang, Y. Tang, H. Li, and X. Li, "A battery/ultra-capacitor hybrid energy storage system for implementing the power management of virtual synchronous generators," *IEEE Trans. Power Electron.*, vol. 33, no. 4, pp. 2820-2824, Apr. 2018.

[6] T. Shintai, Y. Miura, and T. Ise, "Oscillation damping of a distributed generator using a virtual synchronous generator," *IEEE Trans. Power Deliv.*, vol. 29, no. 2, pp. 668-676, Apr. 2014.

[7] W. Ma, Y. Guan, and B. Zhang, "Active disturbance rejection control based control strategy for virtual synchronous generators," *IEEE Trans. Energy Convers.*, vol. 35, no. 4, pp. 1747-1761, May 2020.

[8] H. Wu, X. Ruan, D. Yang, X. Chen, W. Zhao, Z. Lv, and Q. Zhong, "Small-signal modeling and parameters design for virtual synchronous generators," *IEEE Trans. Power Electron.*, vol. 63, no. 7, pp. 1259-1267, June 2016.

[9] Z. Shuai, C. Shen, X. Liu, Z, Li, and Z. J. Shen, "Transient angle stability of virtual synchronous generators using Lyapunov's direct method," *IEEE Trans. Smart Grid*, vol. 10, no. 4, pp. 4648-4661, July 2019.

[10] J. Chen, T. O' Donnell, "Parameter constraints for virtual synchronous generator considering stability," *IEEE Trans. Power Syst.*, vol. 34, no. 3, pp. 2479-2481, May 2019.

[11] Q. Zhong, "Harmonic droop controller to reduce the voltage harmonics of inverters," *IEEE Trans. Ind. Electron.*, vol. 60, no. 3, pp. 936-945, Mar. 2013.

[12] A. Luo, X. Xu, L. Fang, H. Fang, J. Wu, and C. Wu, "Feedback feed-forward PI-type iterative learning control strategy for hybrid active power filter with injection circuit," *IEEE Trans. Ind. Electron.*, vol. 57, no. 11, pp. 3767-3779, Feb. 2010.

[13] M. M. Hashempour, M. Savaghebi, J. C. Vasquez, and J. M. Guerrero, "A control architecture to coordinate distributed generators and active power filters coexisting in a microgrid," *IEEE Trans. Smart Grid*, vol. 7, no. 5, pp. 2325-2336, Sep. 2016.

[14] J. He, Y. Li, N. R. Zargari, Z. Cheng, R. Ni, and Y. Zhang, "A measurement method to solve a problem of using DG interfacing converters for selective load harmonic filtering," *IEEE Trans. Power Electron.*, vol. 31, no. 3, pp. 1852-1856, Mar. 2016.

[15] D. Campos-Gaona, R. Alzola, J. Monroy-Morales, M. Ordonez, O. AnayaLara, and W. Leithead, "Fast selective harmonic mitigation in multifunctional inverters using internal model controllers and synchronous reference frames," *IEEE Trans. Ind. Electron.*, vol. 64, no. 8, pp. 6338-6349, Mar. 2017.

[16] L. Zhou, S. Liu, Y. Chen, W. Yi, S. Wang, X. Zhou, W. Wu, J. Zhou, C. Xiao, and A. Liu, "Harmonic current and inrush fault current coordinated suppression method for VSG under non-ideal grid condition", *IEEE Trans. Power Electron.*, vol. 36, no. 1, pp. 1030-1042, Jan. 2021.

[17] A. Micallef, M. Apap, C. Spoteri-Staines, J. M. Guerrero, and J. C. Vasquez, "Reactive power sharing and voltage harmonic distortion compensation of droop controlled single phase islanded microgrids," *IEEE Trans. Smart Grid*, vol. 5, no. 3, pp. 1149-1158, May 2014.

[18] A. Micallef, M. Apap, C. Spiteri-Staines, and J. M. Guerrero, "Mitigation of harmonics in grid-connected and islanded microgrids via virtual admittances and impedances," *IEEE Trans. Smart Grid*, vol. 8, no. 2, pp. 651-661, Mar. 2017.

[19] J. He, Y. W. Li, and M. S. Munir, "A flexible harmonic control approach through voltage-controlled DG-grid interfacing converters," *IEEE Trans. Ind. Electron.*, vol. 59, no. 1, pp. 444-455, Jan. 2012.

[20] B. Xie, K. Guo, M. Mao, L. Zhou, T. Liu, Q. Zhang, and G. Hao, "Analysis and improved design of phase compensated proportional resonant controllers for grid-connected inverters in weak grid," *IEEE Trans. Energy Convers.*, vol. 35, no. 3, pp. 1453-1464, Sep. 2020.

[21] J. Adhikari, P. IV, and S. K. Panda, "Reduction of input current harmonic distortions and balancing of output voltages of the vienna rectifier under supply voltage disturbances," *IEEE Trans. Power Electron.*, vol. 32, no. 7, pp. 5802-5812, Jul. 2017.

[22] W-K. Sou, W-H Choi, C-W. Chao, C-S. Lam, C. Gong, C-K. Wong, and M-C. Wong, "A deadbeat current controller of LC-hybrid active power filter for power quality improvement," *IEEE Journal Emerg. Sel. Topics Power Electron.*, vol. 8, no. 4, pp. 3891-3905, Dec. 2020.

[23] Q. Yan, X. Wu, X. Yuan and Y. Geng, "An improved grid-voltage feedforward strategy for high-power three-phase grid-connected inverters based on the simplified repetitive predictor," *IEEE Trans. Power Electron.*, vol. 31, no. 5, pp. 3880-3897, May 2016.

[24] Y. Peng, W. Sun, and F. Deng, "Internal model principle method to robust output voltage tracking control for single-phase UPS inverters with its SPWM implementation", *IEEE Trans. Energy Convers.*, DOI: 10.1109/ TEC.2020.3030894.

[25] W. Wu, L. Zhou, Y. Chen, A. Luo, Y. Dong, X. Zhou, Q. Xu, L. Yang, and J. M. Guerrero, "Sequence-impedance-based stability comparison between VSGs and traditional grid-connected inverters," *IEEE Trans. Power Electron.*, vol. 34, no. 1, pp. 46-52, Jan. 2019.

[26] L. Zhou, Z. Shuai, Y. Chen, W. Wu, X. Zhou, K. Yan and A. Luo, "Impedance-based harmonic current suppression method for VSG connected to distorted grid", *IEEE Trans. Ind. Electron.*, vol. 67, no. 7, pp. 5490-5502, Jul. 2020.

[27] X. Quan, X. Dou, Z. Wu, M. Hu, and F. Chen, "A concise discrete adaptive filter for frequency estimation under distorted three-phase voltage," *IEEE Trans. Power Electron.*, vol. 32, no. 13, pp. 9400-9412, Dec. 2017.

[28] A. Bidram, A. Davoudi, F. L. Liews, and J. M. Guerrero, "Distributed cooperative secondary control of microgrid using feedback linearization," *IEEE Trans. Power Syst.*, vol. 28, no. 3, pp. 3462–3470, Aug. 2013.

[29] G. Lou, Q. Yang, W. Gu, J. Zhang, "An improved control strategy of virtual synchronous generator under symmetrical grid voltage sag," *INT. J. Elec. Power*, DOI: 10.1016/j.ijepes.2020.106093.

Guannan Lou (S'17-M'19) received the B.S. and M.S. degrees in Control Science and Engineering from North China Electric Power University, China, in 2008 and 2011, respectively. From 2011 to 2015, she joined in Guodian Nanjing Automation Co., Ltd, Nanjing. In 2018, she received the Ph.D. degree in Electrical Engineering from Southeast University, China.

From 2017 to 2018, she was a joint Ph.D. student with Argonne National Laboratory. She is currently a Lecturer in the School of Electrical Engineering, Southeast University. Her research interests include distributed generations integration, microgrid modeling and control.

Quan Yang received the B.S. and M.S. degrees in electrical engineering from Southeast University, China in 2017 and 2020, respectively.

He is currently an assistant engineer in Dongguan power supply bureau of Guangdong power grid company, Dongguan, China. His research interests include distributed generations and power quality in microgrids.

Wei Gu (M'06-SM'16) received his B.S. and Ph.D. degrees in Electrical Engineering from Southeast University, China, in 2001 and 2006, respectively.

From 2009 to 2010, he was a Visiting Scholar in the Department of Electrical Engineering, Arizona State University. He is now a professor in the School of Electrical Engineering, Southeast University. He is the director of the institute of distributed generations and active distribution networks. His research interests include distributed generations and microgrids, integrated energy systems.

Dr. Gu is an Editor for the IEEE Transactions on Power Systems, the IET Energy Systems Integration and the Automation of Electric Power Systems (China).

Xiangjun Quan (S'16-M'18) received the B.S and M.S. degrees in electrical engineering from Chongqing University, Chongqing, China, in 2007 and Southeast University, Nanjing, China, in 2014. In 2018, he received his Ph.D.

degree in electrical engineering from Southeast University. From February 2017 to August 2017, he had studied in FREEDM at NC State University. From September 2017 to August 2018, he had also studied in University of Texas at Austin as an exchange student. He was a R&D engineer with Huawei Technologies from 2011 to 2012. Since 2018, he has been an Assistant Professor with Southeast University. His current research interests include digital control technique for converters, renewable energy generation systems and microgrid.

Josep M. Guerrero (S'01-M'04-SM'08-FM'15) received the B.S. degree in telecommunications engineering, the M.S. degree in electronics engineering, and the Ph.D. degree in power electronics from the Technical University of Catalonia, Barcelona, in 1997, 2000 and 2003, respectively. Since 2011, he has been a Full Professor with the Department of Energy Technology, Aalborg University, Denmark, where he is responsible for the Microgrid Research Program. From 2014 he is chair Professor in Shandong University; from 2015 he is a distinguished guest Professor in Hunan University; and from 2016 he is a visiting professor fellow at Aston University, UK, and a guest Professor at the Nanjing University of Posts and Telecommunications. From 2019, he became a Villum Investigator by The Villum Fonden, which supports the Center for Research on Microgrids (CROM) at Aalborg University, being Prof. Guerrero the founder and Director of the same centre (www.crom.et.aau.dk).

His research interests is oriented to different microgrid aspects, including power electronics, distributed energy-storage systems, hierarchical and cooperative control, energy management systems, smart metering and the internet of things for AC/DC microgrid clusters and islanded minigrids. Specially focused on microgrid technologies applied to offshore wind, maritime microgrids for electrical ships, vessels, ferries and seaports, and space microgrids applied to nanosatellites and spacecrafts. Prof. Guerrero is an Associate Editor for a number of IEEE TRANSACTIONS. He has published more than 600 journal papers in the fields of microgrids and renewable energy systems, which are cited more than 60,000 times. He received the best paper award of the IEEE Transactions on Energy Conversion for the period 2014-2015, and the best paper prize of IEEE-PES in 2015. As well, he received the best paper award of the Journal of Power Electronics in 2016. During seven consecutive years, from 2014 to 2020, he was awarded by Clarivate Analytics (former Thomson Reuters) as Highly Cited Researcher with 50 highly cited papers. In 2015 he was elevated as IEEE Fellow for his contributions on "distributed power systems and microgrids."

Shanlin Li received his B.S degree in electrical engineering from Southeast University, Nanjing, China in 2020 and currently he is pursuing his M.S degree. His research interests include distributed generations and microgrids.